



LUND UNIVERSITY

QM/MM study of the stereospecific proton exchange of glutathiohydroxyacetone by glyoxalase I

Jafari, Sonia; Ryde, Ulf; Irani, Mehdi

Published in:
Results in Chemistry

DOI:
[10.1016/j.rechem.2019.100011](https://doi.org/10.1016/j.rechem.2019.100011)

2019

Document Version:
Publisher's PDF, also known as Version of record

[Link to publication](#)

Citation for published version (APA):
Jafari, S., Ryde, U., & Irani, M. (2019). QM/MM study of the stereospecific proton exchange of glutathiohydroxyacetone by glyoxalase I. *Results in Chemistry*, 1, Article 100011. <https://doi.org/10.1016/j.rechem.2019.100011>

Total number of authors:
3

Creative Commons License:
CC BY

General rights

Unless other specific re-use rights are stated the following general rights apply:
Copyright and moral rights for the publications made accessible in the public portal are retained by the authors and/or other copyright owners and it is a condition of accessing publications that users recognise and abide by the legal requirements associated with these rights.

- Users may download and print one copy of any publication from the public portal for the purpose of private study or research.
- You may not further distribute the material or use it for any profit-making activity or commercial gain
- You may freely distribute the URL identifying the publication in the public portal

Read more about Creative commons licenses: <https://creativecommons.org/licenses/>

Take down policy

If you believe that this document breaches copyright please contact us providing details, and we will remove access to the work immediately and investigate your claim.

LUND UNIVERSITY

PO Box 117
221 00 Lund
+46 46-222 00 00



QM/MM study of the stereospecific proton exchange of glutathiohydroxyacetone by glyoxalase I

Sonia Jafari^{a,b}, Ulf Ryde^b, Mehdi Irani^{a,*}

^a Department of Chemistry, University of Kurdistan, P.O. Box 66175-416, Sanandaj, Iran

^b Department of Theoretical Chemistry, Lund University, P. O. Box 124, SE-221 00 Lund, Sweden

ARTICLE INFO

Article history:

Received 23 July 2019

Accepted 10 October 2019

Keywords:

Glyoxalase I

Enantioselectivity

Reaction mechanism

QM/MM

Free energy perturbation

DFT

ABSTRACT

We have performed quantum mechanics (QM), molecular mechanics (MM) and hybrid QM/MM calculations to study the stereospecific proton exchange of glutathiohydroxyacetone (HOC-SG) by glyoxalase I (GlxI). We did the QM/MM calculations with a large QM system (246 atoms) to investigate the proton-exchange mechanism. Moreover, single-point big-QM energies with 1303 atoms in the big QM system and 22,412 atoms in the MM system were used to compare the energy difference of the stationary structures. GlxI catalyzes the exchange of the pro-S, but not the pro-R hydroxymethyl proton of HOC-SG with a deuterium from the D₂O solvent. Classical molecular dynamics simulations with different protonation states of Glu99, Glu172 and HOC-SG led to the determination of most stable species (Glu-172 is protonated and the alcoholic oxygen of HOC-SG is deprotonated). The QM/MM results showed that before binding of HOC-SG, both active-site glutamates are charged, whereas HOC-SG is protonated. When HOC-SG binds, its alcoholic proton (H_O) can point toward either Glu-99 or Glu-172. However, if the substrate binds so that H_O is directed toward Glu-99, it is not transferred, whereas if it is directed toward Glu-172, the latter abstracts H_O. The results showed that transferring H_O to the glutamates from the reactant states is the key step to make the proton exchange reaction possible. Our calculations show that order of basicity of the glutamates and HOC-SG inside the enzyme is: Glu-172 > HOC-SG > Glu-99. The calculations allow us to propose a reaction mechanism for the stereospecific proton exchange of HOC-SG by GlxI with an overall barrier of 14.1 kcal/mol.

© 2019 The Authors. Published by Elsevier Ltd. This is an open access article under the CC BY license (<http://creativecommons.org/licenses/by/4.0/>).

1. Introduction

Enzymes are biological catalysts. Unlike other catalysts, they are usually highly selective and specific for particular chemical reactions. They generally catalyze only one type of reactions; for example, acetylene hydratase catalyzes the non-redox hydration of acetylene in the anaerobic unsaturated hydrocarbon metabolism [1]. Some enzymes are both chemoselective and enantioselective; for example, lipase B from *Candida antarctica* favors the *R* enantiomer of 1-phenylethanol [2]. However, only a few enzymes accept both enantiomers of a chiral substrate but convert them to only one enantiomer of the product [3,4]. The typical example is glyoxalase I (EC 4.4.1.5, lactoylglutathione lyase; GlxI), which converts both enantiomers of its substrate into the same enantiomer of its product [3].

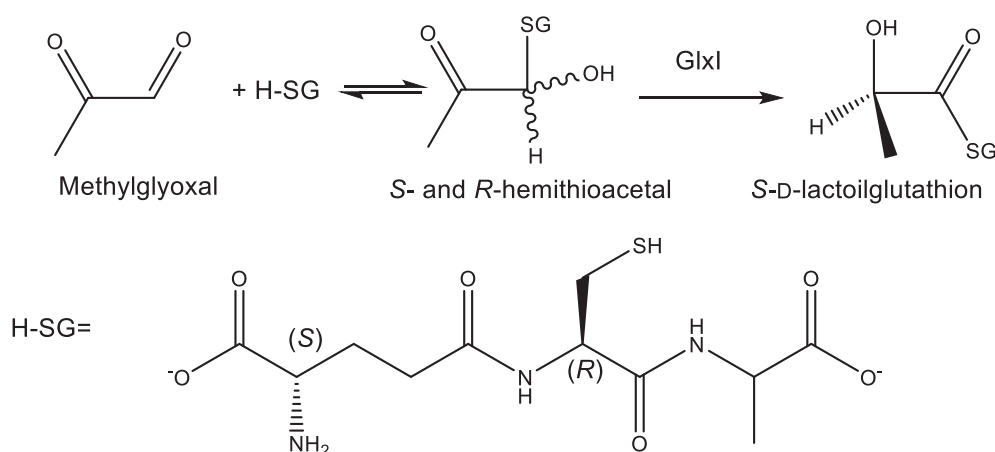
Classically, chemoselectivity and enantioselectivity of enzymes can be related to their large, folded, twisted and entangled tertiary and quaternary structures, which give them unique three-dimensional structures. The catalytic activity of enzymes takes place in a relatively small

region, the active site. The remaining three-dimensional structure provides a skeleton and modulator for the active site, either by imposing a special shape or electron density to the active-site pocket. A simple understanding of the enantioselectivity of enzymes can be gained from a hollow mold model. A left hand cannot be fitted into a hollow mold of a right hand and likewise an *S* enantiomer of a substrate cannot bind to the active site of an enantioselective enzyme that is designed to bind the *R* enantiomer. Of course, this gives a very rough description of enzyme selectivity, neglecting contributions from dynamics and electrostatics effects from the enzymes tertiary and quaternary structures. In addition, it cannot explain selectivity of enzymes with a symmetric active site (e.g. GlxI, the case of this study). On the other hand, computational enzymatic methods can give a detailed and accurate description of enzyme catalysis and selectivity. Such methods have been used to investigate selectivity of some enzymes [5–16]. Herein, we apply quantum mechanics (QM), molecular mechanics (MM) and hybrid QM/MM methods to study the unusual stereospecificity of GlxI.

In the last two decades, different aspects of the catalytic mechanism of GlxI have been studied [3,7,10,17–28]. As shown in Scheme 1, the enzyme accepts both enantiomers of its chiral substrate (hemithioacetals of methylglyoxal with a variety of aromatic and aliphatic α -ketoaldehydes) but gives only one enantiomer of its product (*S*-D-

* Corresponding author.

E-mail addresses: jafarisonia@yahoo.com (S. Jafari), ulf.ryde@teokem.lu.se (U. Ryde), m.irani@uok.ac.ir (M. Irani).



Scheme 1. The reaction catalyzed by GlxI.

lactoylglutathione). Interestingly, crystal structures of the enzyme [22] show a symmetric active site (cf. Fig. 1) with a Zn ion coordinated by Gln-33, His-126, Glu-99 and Glu-172, as well as either two water molecules (Fig. 1a) or an inhibitor (Fig. 1b) [22]. This symmetry can explain why GlxI accepts and converts both S- and R-enantiomers of the substrate. However, it does not explain why the enzyme produces only one enantiomer of the product. On the contrary, we would expect from a symmetric active site to produce both enantiomers of the product and not only one of them. In fact, QM-cluster calculations using rather small models could not explain the unusual stereospecificity of GlxI [10]. This implies that something more complicated takes place inside the enzyme that allows it to produce only one enantiomer of the product. A deeper look at the active site reveals an important asymmetry. Fig. 1b shows that in the crystal structure of an S-[N-hydroxy-N-(p-iodophenyl)carbamoyl]glutathione (HIC-SG) inhibited GlxI, Glu-172 is displaced from the Zn ion, whereas Glu-99 remained coordinated to the ion (the shortest Zn-O distance for the two residues is 3.26 and 1.90 Å, respectively).

Two experimental facts confirm the asymmetry of the active-site glutamate residues: i) Glu-172 or Glu-99 initiate the catalytic reaction of GlxI by abstracting the H1 atom from the S- or R-substrate, respectively (cf. Scheme 2 for the naming of atoms) [22,25–27]. However, experiments showed that isomerization of R- and S-glutathiolactaldehydes by GlxI is characterized by a nonstereospecific

proton abstraction followed by a partially shielded proton transfer to the *si* face of the cis-enediol intermediate [3]. ii) GlxI exclusively catalyzes the exchange of the pro-S (H_S), but not the pro-R (H_R) hydroxymethyl proton of a product analogue (glutathiohydroxyacetone; HOC-SG) with deuterium from the D_2O solvent (Scheme 3). In addition, the enzyme mediates the exchange of the pro-S, but not pro-R hydroxymethyl deuterium of [2H]-HOC-SG with a proton from the H_2O solvent [20].

HOC-SG is not the normal substrate of GlxI, but based on experimental observations, Creighton and Hamilton proposed that a substrate analogue is processed in the same way as the normal substrate [27]. Considering this fact, we recently studied the proton-exchange reaction of HOC-SG by GlxI (the reaction shown in Scheme 3) [7]. We employed the QM-cluster approach [29] and classical molecular dynamics (MD) simulations. The results indicated that the unusual stereospecificity of GlxI is caused by the more flexible environment of Glu-172 compared to that of Glu-99 [7]. We used the higher flexibility of Glu-172 to justify the higher basicity of it, which was proposed by Cameron et al. [22] i.e. the higher flexibility of Glu-172 allows it to dissociate from the active-site Zn ion and then attain a higher basicity. The higher flexibility and basicity of Glu-172 allow it to abstract and transfer protons much easier than Glu-99 in the catalytic reaction [7].

Several lines of evidence indicate that Glu-172 is protonated in the crystal structure and in the HOC-SG bounded enzyme: i) In the HIC-SG

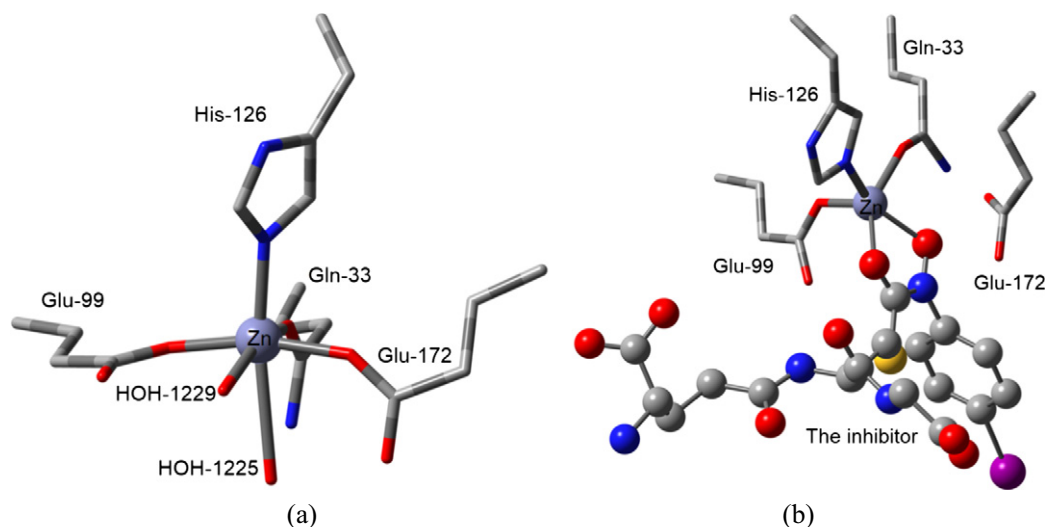
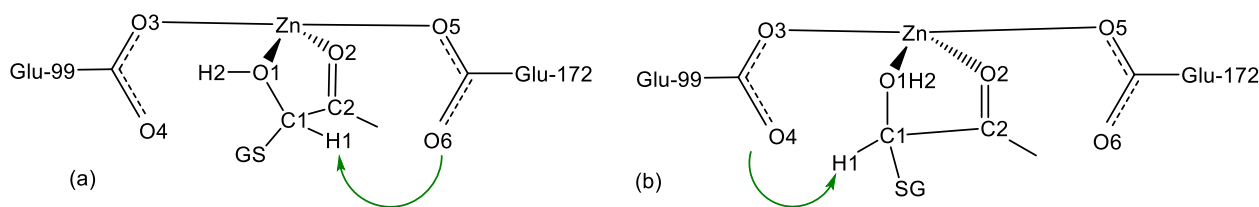


Fig. 1. The active site of GlxI from crystal structures (a) without any bounded substrate (1QIP PDB ID) or (b) with a bound inhibitor (1QIN PDB ID). Residues are shown up to the CA atoms. The Zn ion and the inhibitor are shown in balls, whereas the normal residues are shown as tubes.



Scheme 2. The proposed initial step of the GlxI reaction, showing that (a) Glu-172 abstracts H1 from the S-substrate and (b) Glu-99 abstracts H1 from the R-substrate.

(this molecule has a similar structure to HOC-SG) bounded crystal structure of GlxI [22], the inhibitor is directly coordinated to the Zn ion, displacing Glu-172. It is well known that metals lower the pK_a of their ligands. For example, the pK_a value of water in aqueous metal complexes is reduced from 15.7 for bulk water to 12.8 and 2.2 for Ca^{2+} and Fe^{3+} , respectively [30]. Therefore, it is possible that HIC-SG is deprotonated and a proton may actually reside on the dissociated Glu-172. ii) QM-cluster calculations starting from the 1QIN crystal structure and with the normal substrate of GlxI show that Glu-172 is protonated but not Glu-99 in reactant states [7,10]. iii) Calculations starting from a crystal structure with a rather symmetric active site [21] show that if the two glutamate ligands are free to move during the optimization, the protonated Glu-172 will dissociate from the zinc ion [25].

Despite all studies, there still are no quantitative calculations of the amount of basicity of the glutamate residues. In this paper, we extrapolate these hypotheses to a HOC-SG bounded GlxI and use QM/MM methods to investigate if HOC-SG is negatively charged or neutral in the enzyme and if its protonation state depends on the conformation of its alcoholic group. Then, we compare computationally the basicity of the glutamate residues and the bound substrate. Moreover, we also determine a reaction path for the proton-exchange reaction and study how it is affected by the conformation of HOC-SG in the enzyme.

2. Methods

2.1. The protein

All calculations are based on the 2.0 Å crystal structure of human GlxI (PDB code 1QIN) [22], which is composed of two identical and entangled subunits each with 183 residues, two Zn ions and two HIC-SG molecules. This structure was selected because it contains the intermediate analogue (HIC-SG) bound to the active site, which resembles binding of HOC-SG (cf. Fig. 2). The experimental data come from yeast GlxI, but there is no crystal structure for GlxI of this organism. However, Aronsson et al. showed that GlxI from both human and yeast contains one zinc ion per active site [31]. Therefore, we used the crystal structure of native human GlxI to model the reaction [22]. Both subunits and all crystal-water molecules were included in the calculations.

We study the reaction of the product analogue HOC-SG and we built it from the enediolate intermediate analogue (HIC-SG), which is located at the active sites and coordinates to the Zn ion. These two compounds have very similar structures and sizes (cf. Fig. 2) and HOC-SG fits nicely into the active site pocket at the same position as HIC-SG. The replacement was done in both active sites for the MD simulations, whereas for the QM/MM calculations the replacement was done in only one of

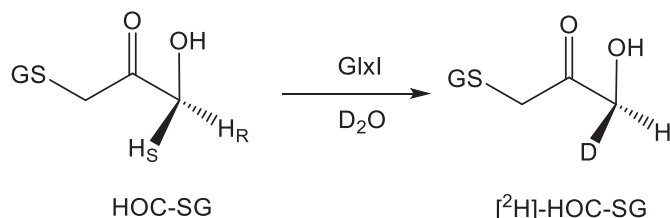
the active sites and in the other active site, the inhibitor was replaced with two water molecules coordinated to the Zn ion. Thus, the reaction was assumed to take place only in one active site, whereas the other site was a spectator. There is no experimental evidence for any cooperativity between the two active sites [3,7,10,17–28]. The same QM/MM approach has successfully been used for other enzymes [32,33].

The protonation states of all the residues were determined by a study of the hydrogen-bond pattern, the solvent accessibility and the possible formation of ionic pairs. They were also checked by PROPKA calculations [34]. See the Supporting Information for details of the protonation states.

2.2. MD simulations

The MD simulations were performed using the GPU-accelerated *pmemd* code [35–37] of AMBER 16 [38]. The protein and HOC-SG were described with the Amber ff14SB [39] and GAFF [40] force fields, respectively. Water molecules were described explicitly using the TIP3P model [41]. The Zn sites were treated by a non-bonded model with restraints between the metal and the ligands [42], implemented as NMR bond restraints (nmropt = 1 option and &rst name lists; a restraints file is given in the Supporting Information). For the restraints, we used the metal–ligand distances observed in the crystal structure (averaged over the two subunits). In addition, for the metal sites, RESP charges were employed [43], fitted to electrostatic potentials calculated and sampled with the Merz–Kollman scheme [44]. The force constants and RESP charges were obtained from the optimized models in Fig. S1 in the Supporting Information. These calculations were performed at B3LYP-D3/def2-SV(P) [45–50] level of theory, using the Turbomole software (version 7.1) [51]. The force constants were calculated by the method of Seminario [52,53] and averaged over interactions of the same types. The calculated force constants and charges are given in Tables S1–S3 in the Supporting Information. The Amber ff14SB force field employs charges, calculated with the Hartree–Fock method, but it is well-known that metal-sites are poorly described at the Hartree–Fock level of theory. Therefore, we prefer to obtain the charges with a DFT level of theory with significant amount of Hartree–Fock exchange [54].

The setup of the MD simulations is similar to that in our recent works [7,55]. The enzyme was solvated in a periodic truncated octahedral box of TIP3P water molecules, extending at least 14 Å from the solute using the



Scheme 3. The stereospecific proton exchange of HOC-SG, catalyzed by GlxI.

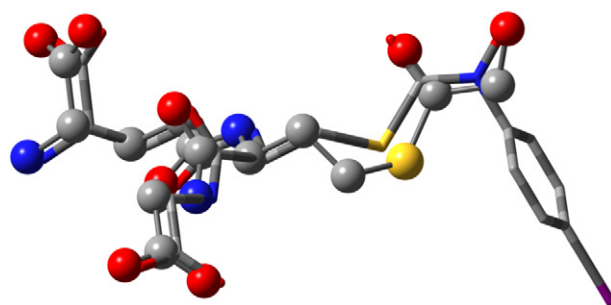


Fig. 2. Superposition of HOC-SG and HIC-SG from the crystal structure, showing the similarity in size and shape of the two molecules. HOC-SG and HIC-SG are shown in balls and tubes, respectively. Hydrogen atoms are omitted for clarity.

tleap program in the Amber suite [38]. No counter ions were added to any of the systems. The final system contained ~44,680 atoms. After the solvation, the systems were subjected to 1000 cycles of minimization, with the heavy atoms of the protein restrained toward the starting structure with a force constant of 100 kcal/mol/Å². This was followed by a 20 ps constant-volume and a 20 ps constant-pressure equilibration with the same restraints, but a force constant of 50 kcal/mol/Å². Finally, the systems were equilibrated for 1 ns without any restraints, followed by a 300 ns production simulation, during which coordinates were sampled every 10 ps. The temperature was kept constant at 300 K using Langevin dynamics with a collision frequency of 2 ps⁻¹ [56]. The pressure was kept constant at 1 atm using Berendsen's weak coupling isotropic algorithm with a relaxation time of 1 ps [57]. Long-range electrostatics were handled by particle-mesh Ewald summation [58] with a fourth-order B spline interpolation and a tolerance of 10⁻⁵. The cut-off radius for Lennard-Jones interactions was set to 8 Å. All bonds involving hydrogen atoms were constrained to their equilibrium values using the SHAKE algorithm [59], allowing for a time step of 2 fs during the simulations. The root-mean-square deviation (RMSD) was calculated with the AMBER *cptraj* module [60], analyzing trajectories with coordinates which were saved every 10 ps and using the crystal structure as the reference. The reported values are averages over 30,000 sets of coordinates.

For the QM/MM calculations, the protein was instead solvated in a sphere with a radius of 40 Å around the geometrical center of the protein. The final system contained ~23,700 atoms. The positions of the added protons and water molecules, as well as all atoms of HOC-SG were optimized in 100 steps of steepest descent minimization, keeping all other heavy atoms fixed at the crystal-structure positions. This allowed the substrate to relax in the active site (it was inserted manually into the enzyme). Then, the added protons and water molecules were optimized by a 240 ps simulated annealing calculation (up to 370 K), followed by a 1000 steps minimization, keeping the other atoms fixed at the crystal-structure positions. No SHAKE restraints were employed and the time step was 0.5 fs.

2.3. QM/MM calculations

The QM/MM calculations were performed with the ComQum software [61,62]. In this approach [63,64], the protein and solvent are split

into three subsystems: System 1 (the QM region) was treated by QM methods. System 2 consisted of all residues or water molecules within 6 Å of any atom in system 1. In some calculations (called protein-fixed), system 2 was kept fixed at the original (crystallographic) coordinates. Such calculations were run to ensure that the surroundings residues are in the same local minimum in all calculations, making the energies stable, although all outer-sphere reorganization is ignored. In other calculations (called protein-free), all residues and solvent molecules in system 2 were allowed to relax by a full MM minimization in each cycle of the QM optimization. Note also that the full protein is relaxed in the QM/MM calculations (see below). Finally, system 3 contained the remaining part of the protein and the solvent. It was kept fixed at the original coordinates (equilibrated crystal structure).

In the QM calculations, system 1 was represented by a wave function, whereas all the other atoms were represented by an array of partial point charges, one for each atom, taken from MM libraries. Thereby, the polarization of the QM system by the surroundings is included in a self-consistent manner. When there is a bond between systems 1 and 2 (a junction), the hydrogen link-atom approach was employed. In this approach, the QM system was capped with hydrogen atoms (hydrogen link atoms, HL), the positions of which are linearly related to the corresponding carbon atoms (carbon link atoms, CL) in the full system [61,65]. All atoms were included in the point-charge model, except the CL atoms [66]. The point charges do not necessarily sum up to an integer, because the Amber force field does not employ charge groups [67]. The total QM/MM energy in ComQum was calculated as [61,62],

$$E_{\text{QM/MM}} = E_{\text{QM1+ptch23}}^{\text{HL}} + E_{\text{MM123,q1=0}}^{\text{CL}} - E_{\text{MM1,q1=0}}^{\text{HL}} \quad (1)$$

where $E_{\text{QM1+ptch23}}^{\text{HL}}$ is the QM energy of system 1, truncated by HL atoms and embedded in the set of point charges representing systems 2 and 3 (but excluding the self-energy of the point charges). $E_{\text{MM1,q1=0}}^{\text{HL}}$ is the MM energy of the QM system, still truncated by HL atoms, but without any electrostatic interactions. Finally, $E_{\text{MM123,q1=0}}^{\text{CL}}$ is the classical energy of all atoms in the system with CL atoms and with the charges of the QM system set to zero (to avoid double counting of the electrostatic interactions). By using this approach, which is similar to the one used in the Oniom method [68], errors caused by the truncation of the quantum

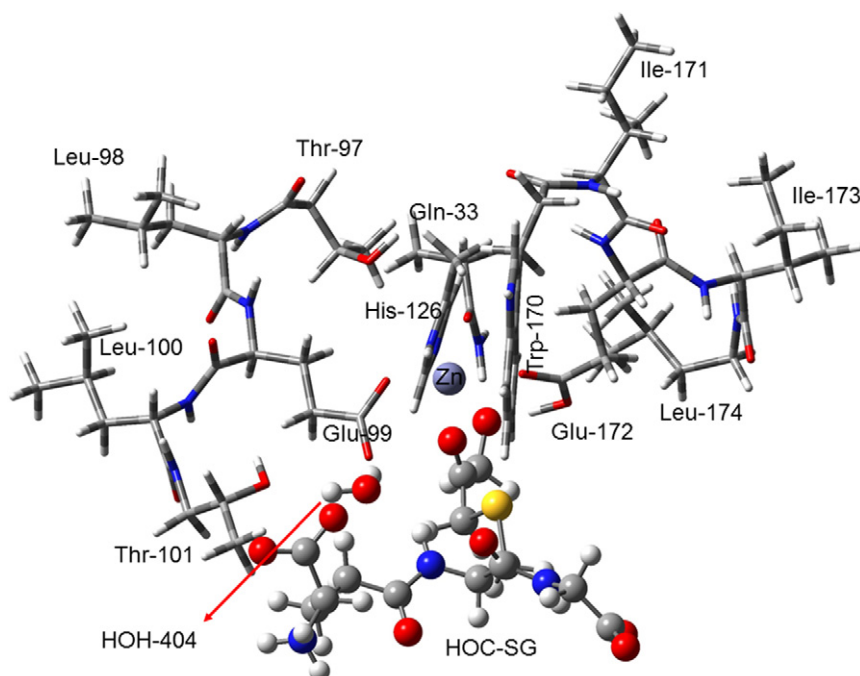


Fig. 3. The QM system used in the QM/MM calculations. HOC-SG, the Zn ion and HOH-404 are shown in a ball-and-stick representation and the protein residues are shown as tubes.

system should partly cancel out. Thus, ComQum employs a subtractive scheme with electrostatic embedding and van der Waals link-atom corrections [69].

The QM/MM geometry optimizations were performed using the Turbomole software [51] at the TPSS/def2-SV(P) level of theory [50,70]. The calculations were sped up by expanding the Coulomb interactions in an auxiliary basis set, the resolution-of-identity approximation [71,72] and empirical dispersion corrections were included with the DFT-D3 approach [48] and Becke–Johnson damping [49] as implemented in Turbomole. The MM calculations were performed with the Amber software [67], using the Amber ff14SB [39] and GAFF [40] force fields for the protein and HOC-SG, respectively. Water molecules were described by the TIP3P model [41].

All first-order stationary states (reactants, products and intermediates) were fully optimized without any restraints. To go from one first-order stationary point to another, we moved a proton step by step, applying either an H–O or a H–C restraint with a force constant of 1 a.u. and changing the corresponding target value in steps of 0.2 Å (0.1 Å around the maximum in energy). For example, going from **IM1** to **IM2**, we scanned the H_R–O1 distance in 11 steps. In each step, all other degrees of freedom were optimized. The transition states were approximated as the highest point on the potential energy surface along the reaction coordinates. Scans were performed in both directions, i.e. both from the reactant and from the product, to ensure that the paths are connected and that the hysteresis is minor. Forward and backward reaction profiles are compared in Fig. S2 in the Supporting Information.

The QM system consisted of the Zn ion, models of Gln-33 and His-126 (the glutamine was represented by propanamide and histidine by methyl-imidazole), and all atoms of Thr-97, Leu-98, Glu-99, Leu-100, Thr-101, Trp-170, Ile-171, Glu-172, Ile-173, Leu-174, HOC-SG and HOH-404 (cf. Fig. 3), giving a total of 246 atoms. The QM/MM calculations were performed when system 2 was fixed at the crystallographic coordinates.

We have also performed a large amount of preliminary calculations with 10 other QM systems. Those QM/MM calculations were performed when system 2 was either fixed or free to relax. The calculations led us to choose a proper QM system. The results are collected in the Supporting information.

2.4. Big-QM calculation

Previous studies have shown that QM/MM energies strongly depend on the size of the studied QM system [66,73]. Neutral residues have a significant effect on energies only when they are within 4.5 Å of the active site [66] but all buried charges in the protein significantly affect the energies [66,73]. Moreover, QM/MM calculations are sensitive to locations of the junctions between the MM and QM system [64,66]. Therefore, we have developed the big-QM method which moves the junctions 2–3 residues away from the QM system and includes all charged residues and all residues with at least one atom within 4.5 Å of any atom in the original QM system [74,75].

In this work, our big-QM system consisted of all chemically reasonable groups (i.e. keeping functional groups, as well as conjugated and aromatic systems intact) with at least one atom within 4.5 Å of any atom in the QM system shown in Fig. 3. Moreover, all junctions were moved at least three residues away from the QM system. There is only one buried charge group in GlxI that is neither in the QM systems nor is coordinated to a metal ion (Arg-37). This group was also included in the big-QM system. This gave a system of 1303 atoms, shown in Fig. 4. The big QM energy calculations were performed on the QM/MM optimized structures. The calculations were performed as described above, but they employed also the multipole-accelerated resolution-of-identity *J* approach (*marij* keyword) [76]. The calculations were run with the parallel version of Turbomole [77]. To the big-QM energies, we added the DFT-D3 dispersion correction and a MM correction (

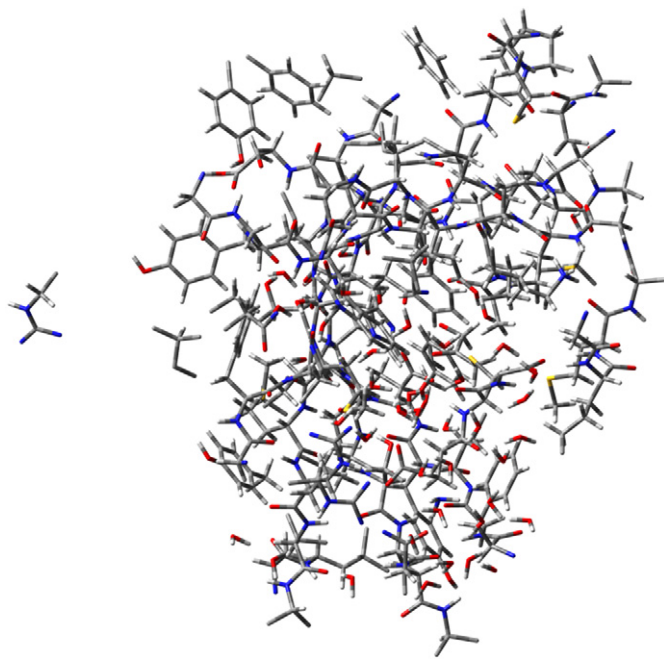
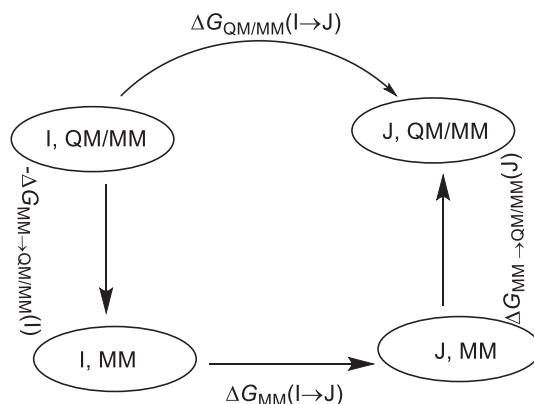


Fig. 4. Atoms included in the big-QM system.

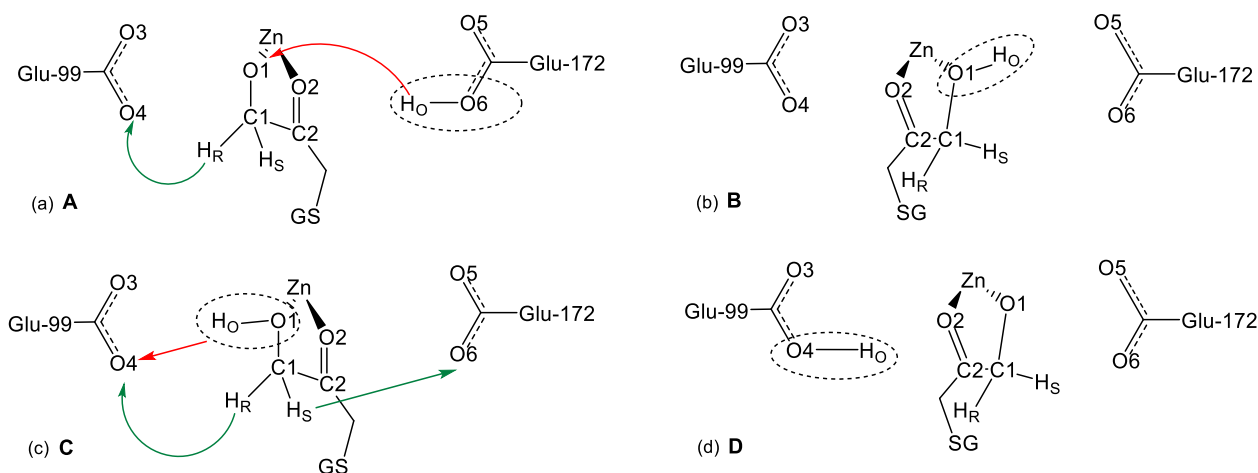
$E_{\text{MM123},q_1=0}^{\text{CL}} - E_{\text{MM1},q_1=0}^{\text{HL}}$), yielding a standard QM/MM energy but with the big-QM system as the QM region.

2.5. QM/MM-PBSA calculations

The QM/MM-PBSA method [78,79] can be viewed as a post-processing of QM/MM calculations to obtain more stable energies, including a solvation term obtained by continuum methods. It is an adaptation of the widely used MM/PBSA approach [80,81] for QM/MM calculations. Two variants of QM/MM-PBSA were used. They differ in how the QM energy and the charges on the QM atoms are calculated [33,78,82]. In the first approach, denoted by Vac in the following, the QM energy and the charges were calculated from a vacuum wave function. In the second approach, denoted Ptch below, the QM wave function is obtained with a point-charge model of the MM system. The calculations were automatized and performed by Linux shell scripts, which are available from the authors on request. Further details of the QM/MM-PBSA calculations can be found in the Supporting Information and in http://www.teokem.lu.se/~ulf/Methods/qmmm_pbsa.html.



Scheme 4. The thermodynamic cycle employed in the QTCF calculations.



Scheme 5. Schematic views of the protonation states of the glutamates and HOC-SG in the simulations. **B** and **C** represent the H_0 to172 and H_0 to99 conformations, respectively.

2.6. QTCP calculations

The QTCP approach (QM/MM thermodynamic cycle perturbation) is a method to calculate free energies between two states, I and J, with a high-level QM/MM method, using free-energy perturbation (FEP) with sampling at only the MM level [83–85]. It employs the thermodynamic cycle shown in Scheme 4, showing that the QM/MM free-energy difference between I and J can be obtained from three calculations: an FEP from I to J at the MM level and two FEP calculations in method space from MM to QM/MM, one each for the I and the J states.

$$\Delta G_{\text{QM/MM}}(I \rightarrow J) = \Delta G_{\text{MM}}(I \rightarrow J) - \Delta G_{\text{MM} \rightarrow \text{QM/MM}}(I) + \Delta G_{\text{MM} \rightarrow \text{QM/MM}}(J) \quad (2)$$

The QTCP calculations were performed as has been described before [33,85]. First, each state of interest was optimized by QM/MM, keeping systems 2 and 3 fixed at the crystal structure. Then, the protein was further solvated in an octahedral box of TIP3P water molecules, extending at least 9 Å from the QM/MM system. For the reactant state, the system was subjected to a 1000-step minimization, keeping the atoms in the QM part fixed and restraining all heavy atoms from the crystal structure with a force constant of 100 kcal/mol/Å². Then, two 20 ps MD simulations were run with the heavy atoms still restrained. The first was run with a constant volume, the second with a constant pressure. Next, a 100-ps MD simulation with a constant pressure equilibrated the size of the periodic box and only the heavy atoms in the QM system restrained to the QM/MM structure. The final structure of this simulation was used as the starting structure also for the other state. Finally, an equilibration of 200 ps and a production of 400 ps were run with a constant volume for each state. During the production run, 200 snapshots were collected every 2 ps.

Based on these 200 snapshots, three sets of FEPs were performed as is shown in Scheme 4. First, FEPs were performed at the MM level in the forward and reverse direction along the reaction coordinate by changing the charges and coordinates of the QM system to those of the QM/MM calculations [33]. Charges were first modified in nine steps, keeping the coordinates at those of the reactant state. Then, the coordinates

were modified in five steps to those of the product state (with the charges in the product state). Finally, MM \rightarrow QM/MM FEPs were performed for both the reactant and product states, keeping the QM systems fixed, as has been described before [84,85]. All FEP calculations were performed with the local software *calcqtcp*. Further details of the QTCP calculations can be found in <http://signe.teokem.lu.se/~ulf/Methods/qtcp.html>.

3. Results and discussion

The results are presented in three subsections. First, we describe our tests made to decide a proper protonation state and conformation of the alcoholic oxygen of HOC-SG (O1), Glu-99 and Glu-172 in the active site. Then, we investigate the reaction mechanism for the proton exchange of HOC-SG with QM/MM methods in the enzyme. Finally, we will discuss the flexibility of the glutamates during the obtained reaction path.

3.1. Protonation states of the active site glutamates and HOC-SG

We have performed classical MD simulations and QM/MM calculations to determine the most favorable protonation states of the active site glutamates and HOC-SG. The alcoholic hydrogen atom of HOC-SG, called H_0 in the following, can form a hydrogen bond to the carboxylate group of either Glu-99 or Glu-172. We will call these states the H_0 to99 and H_0 to172 conformations, respectively (shown in Scheme 5c and b, respectively). Alternatively, the H_0 atom may be transferred to the carboxylate groups of either of the glutamates, giving a deprotonated substrate and a protonated Glu-99 or Glu-172 (Scheme 5d and a, respectively). Thus, four conformations are possible and we call them **A**, **B**, **C** and **D** states as is summarized in Table 1 and shown in Scheme 5.

We have performed 300 ns MD simulations for each of these four protonation states. Then, we calculated mass weighted RMSDs from the starting crystal structure for the heavy atoms of Glu-99 and Glu-172, as has been done before for His residues in three proteins [86]

Table 1
Protonation states of the glutamates and HOC-SG in the MD simulations.

	Glu-99 protonation state	Glu-172 protonation state	HOC-SG protonation state	HOC-SG conformation
A	Deprotonated	Protonated	Deprotonated	–
B	Deprotonated	Deprotonated	Protonated	H_0 to172
C	Deprotonated	Deprotonated	Protonated	H_0 to99
D	Protonated	Deprotonated	Deprotonated	–

Table 2
Mass-weighted RMSD values (Å) of the two active-site glutamate residues for the four MD simulations differing in the protonation state (cf. Table 1). Glu-99A and Glu-172B belong to active site 1 and Glu-99B and Glu-172A belong to active site 2. Plots of the time dependence of the RMSDs are shown in Figs. S7–10 in the Supporting Information.

	Active site 1		Active site 2	
	Glu-99A	Glu-172B	Glu-99B	Glu-172A
A	0.49	0.43	0.40	0.58
B	0.33	0.91	0.38	0.97
C	0.37	0.89	0.40	0.92
D	0.28	1.03	0.30	1.06

Table 3

Energy difference in kcal/mol between the **A** and the other protonation states (**B**, **C**, and **D**), calculated by QM/MM, Big-QM, QM/MM-PBSA and QTCP methods.

	QM/MM	Big-QM	QM/MM-PBSA		QTCP
			Vac	Ptch	
A	0.0	0.0	0.0	0.0	0.0
B ^a	2.5	1.2	0.5	0.7	1.2 ± 0.4
C	5.6	4.2	8.0	6.2	3.8 ± 0.5
D ^a	9.4	9.1	9.5	7.8	7.5 ± 0.6

^a No QM/MM local minima were found for the **B** and **D** states; their energies calculated when the distance between H_O and carboxylate group of the corresponding Glu residue was constrained to 1.0 Å.

and for homocitrate and nearby residues in nitrogenase [55]. The RMSD of heavy atoms from the crystal structure gives information about which protonation state is more realistic. The philosophy is that if an incorrect protonation state is employed, the atoms in that residue or in nearby residues will move to release steric or electrostatic clashes or to form new favorable interactions [86]. Therefore, the RMSD will be higher for incorrect protonation states (provided that the reference structure is representative for the state studied).

The calculated RMSDs are summarized in Table 2. It can be seen that the RMSD of Glu-99 does not vary significantly in the four simulations and two subunits (0.28–0.49 Å; cf. Table 2). However, RMSDs of the Glu-172 residue are much lower in the **A** state simulation than in the others (0.43 and 0.58 compared to 0.89–1.06 Å). Thus, the MD results indicate that Glu-172 is probably protonated and HOC-SG is deprotonated (owing to the lower RMSD of this residue in the **A** state simulation) in the HOC-SG bounded enzyme. The differences between the two active sites give an impression of the precision of the results. They are 0.02–0.03 Å for most of the protonation states, but up to 0.06 Å for the **B** state and 0.09–0.15 Å for the **A** state.

To obtain further support for the preferred protonation state of the glutamate residues and HOC-SG, we performed also QM/MM, big-QM, QM/MM-PBSA and QTCP calculations for the four states shown in Scheme 5. The calculated relative energies are collected in Table 3. All methods suggest that **A** is the most stable protonation state, whereas the **D** state is very unstable (7–9 kcal/mol less stable than the **A** state). Moreover, we could not find any QM/MM local minima for the **B** and **D** states (the energies of these states in Table 3 were calculated when

the distance between H_O and the carboxylate group of the corresponding Glu residue was constrained to 1.0 Å).

Thus, our results suggest the following scenario for the binding of HOC-SG to the GlxI: Before the binding, both active-site Glu residues are deprotonated and therefore negatively charged, whereas HOC-SG is protonated. When HOC-SG binds, the proton can point toward either Glu-99 or Glu-172, i.e. the H_Oto99 or H_Oto172 conformations to the active site. However, our calculations show that in the H_Oto172 conformation, the alcoholic proton is abstracted by Glu-172 resulting in the **A** state, whereas in the H_Oto99 conformation, the proton stays on HOC-SG (state **C**).

3.2. Reaction paths

Next, we performed QM/MM calculations with a large QM system (246 atoms) to investigate the proton-exchange mechanism of HOC-SG by GlxI. This method includes electrostatic effects of the surroundings in a self-consistent manner in the wave function, which is more realistic than the implicit surrounding in QM-cluster calculations. Moreover, single-point big-QM energies with 1303 atoms in the QM system were used to compare the energy difference of the stationary structures along the reaction path. These would give a more reliable reaction path than that of the previous QM-cluster calculations [7]. The energies discussed in Sections 3.2.1 and 3.2.2 and the reaction energy profile in Fig. 5 are based on the big-QM energies. The corresponding QM/MM and QTCP results are shown in Fig. S11 in the Supporting Information (they give a similar reaction profile).

Among the protons of the substrate analogue, H_O can be exchanged noncatalytically by a deuterium (it is an alcoholic proton and can be exchanged by a deuterium from D₂O in the reaction medium). Therefore, we suppose that H_O has already been exchanged by a deuterium atom before entering the enzyme active site. In the following, we examine how the protein manages to exchange this proton with H_S, but not with H_R (atom names are shown in Scheme 5).

3.2.1. Reaction paths from the H_Oto99 conformation

As described in the previous section, the most stable state of the H_Oto99 conformation is **C**, in which H_O is on O1 of HOC-SG and is directed toward Glu-99. The schematic structure of the **C** state is shown in Scheme 5c. Starting from the **C** state, there are three possible proton

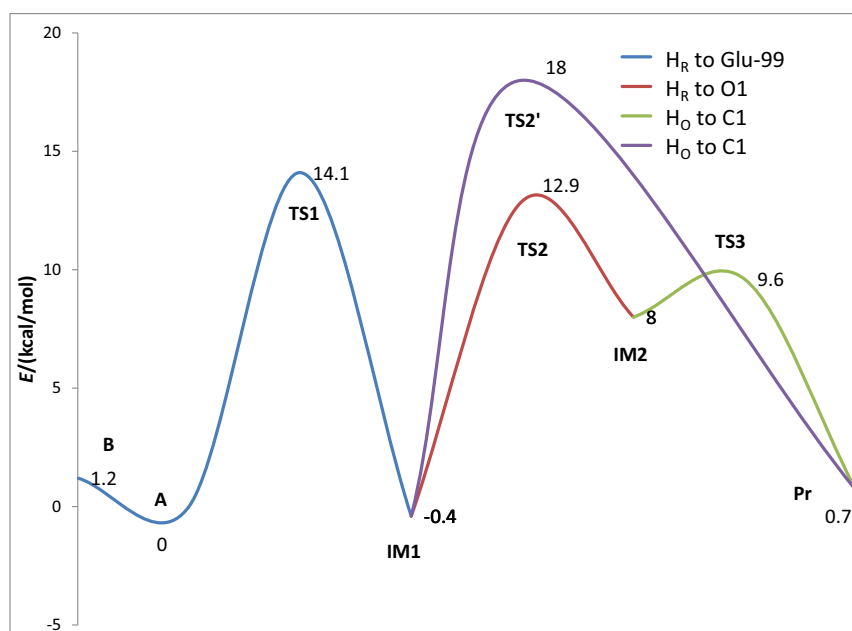


Fig. 5. The big-QM energy profiles from **Re** to **Pr**.

transfers (H_O and H_R to Glu-99 and H_S to Glu-172; these are represented by arrows in Scheme 5c). Our calculations showed that H_O could not move to Glu-99 in the first step for the H_O to99 conformation (the proton transfer shown by a red arrow in Scheme 5c). This would produce the **D** state, which is unstable and can only be obtained when the H_O and Glu-99 distance be constrained. The second proton transfer (H_R to Glu-99) resulted in the structure that is shown in Scheme 6a. From the resulting state shown in Scheme 6a, there are two possible proton transfers (H_S to Glu172 and H_R to C1). The former transfer is unlikely because it would lead to a two-coordinated C1 atom which energetically is not feasible (the transfer shown by the red arrow in Scheme 6a) and the later will go back to the **C** state (the transfer shown by the green arrow in Scheme 6a). Therefore, this path was not tested.

The third proton transfer from the **C** state (H_S to Glu-172) produced the structure shown in Scheme 6b. The barrier and reaction energy for this step was 5.3 and 3.9 kcal/mol, respectively. As can be seen from Scheme 6b there is only one reasonable proton transfer from this structure (H_O to Glu-99; the transfer shown by a red arrow in Scheme 6b). This proton transfer was unsuccessful (H_O returned to the starting point on O1). In conclusion, there is no path for the H_O to99 conformation to exchange H_S by a deuterium.

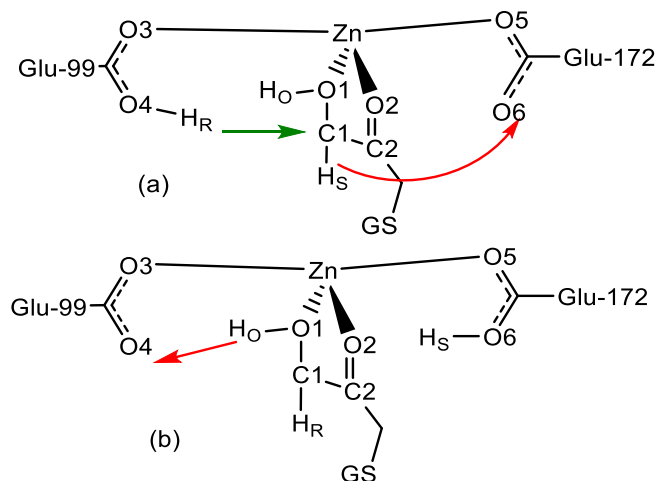
3.2.2. Reaction paths from the H_O to172 conformation

For the H_O to172 conformation, we started the calculations from the **A** protonation state in Scheme 5a, because the results in section 3.1 showed that when HOC-SG binds in the H_O to172 conformation to the enzyme, its alcoholic proton is abstracted by Glu-172, resulting in the **A** state. Starting from the **A** state, there are two reasonable proton transfers (H_O to O1 and H_R to Glu-99; these are represented by arrows in Scheme 5a). Our calculations showed that H_O could not move to O1 in the first step (the proton transfer shown by a red arrow in Scheme 5a); this would produce the **B** state, which is 1.2 kcal/mol less stable than **A** and can only be obtained if the H_O and O1 distance is constrained. The second proton transfer (H_R to Glu-99) would result in the structure that is shown in Scheme 7a (**IM1**). The energy barrier for this step is 14.1 kcal/mol and **IM1** is 0.4 kcal/mol more stable than the **A** state (cf. Fig. 5 for the energies). The barrier for this proton abstraction is 8.8 kcal/mol higher than the corresponding proton abstraction from the **C** state (H_S from C1 by Glu-172 in the **C** state; 14.1 vs 5.3 kcal/mol). This shows that Glu-172 is a stronger nucleophile than Glu-99 (the nucleophiles in the **C** and **A** states are Glu-172 and Glu-99, respectively).

From **IM1**, there are two reasonable proton transfers (H_R to O1 and H_O to C1; the transfers are shown by arrows in Scheme 7a). The results showed that the barrier of the former transfer is 13.3 kcal/mol and reaches to a second intermediate (**IM2**; the structure is shown in Scheme 7b) which is 8.4 kcal/mol higher than **IM1**. From **IM2** there is only one reasonable proton transfer (H_O to C1; shown by an arrow in Scheme 7b). This transfer leaves a product in which H_S is exchanged by H_O (**Pr**; shown in Scheme 7c), in agreement with experimental findings (we supposed that H_O was previously exchange by a deuterium before entering HOC-SG to the active site). This step has a low barrier (1.6 kcal/mol). The **Pr** state is a variant of the **C** state in Scheme 5c in which H_R , H_S and H_O are replaced by H_S , H_O and H_R , respectively (compare the structures of Scheme 5c and Scheme 7c). The two states are almost degenerate (**C** is only 0.8 kcal/mol higher than **Pr**).

Our results showed that the other transfer from the **IM1** state (H_O to C1; shown by a bold green arrow in Scheme 7a) directly reaches to the **Pr** state (H_R simultaneously moves to O1 while moving H_O to C1). However, this proton transfer has a quite high barrier of 18.4 kcal/mol.

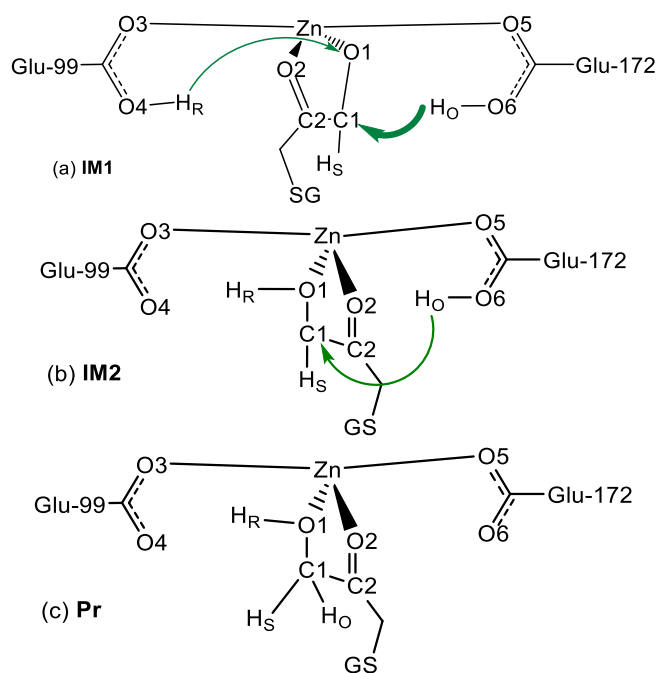
According to the results, there is no path from the H_O to99 conformation of HOC-SG to exchange its H_S by a deuterium. On the other hand, there are two alternative paths from the H_O to172 conformation to a proton exchanged product (**B** → **A** → **IM1** → **IM2** → **Pr** and **B** → **A** → **IM1** → **Pr**). The former has a lower overall barrier (14.1 vs. 18.0 kcal/



Scheme 6. Schematic views and possible proton transfers of the structures resulted from transferring (a) H_R to Glu-99 and (b) H_S to Glu-172 from the **C** state.

mol; cf. Fig. 5), which would make it ~5000 times faster than the later (using the Arrhenius equation at 300 K). Thus, the second path is unlikely. The calculated overall energy barriers are in reasonable agreement with the observed solvent exchange rate constant [20] ($k = 1 \text{ s}^{-1}$, corresponding to an activation barrier of ~17 kcal/mol).

Based on the results, we propose a mechanism for the stereospecific proton exchange of HOC-SG by GlxI as is shown in Scheme 8. First, HOC-SG exchanges non-catalytically its alcoholic proton with a deuterium from the solvent, before entering to the active site. Next, the substrate binds to the enzyme, giving either the **B** or **C** state. The later does not accomplish any path to reach the proton exchanged product. However, the former passes the deuterium to Glu-172, resulting the **A** state. Then, H_R is abstracted by Glu-99, resulting **IM1** (this is the rate determining step with a barrier of 14.1 kcal/mol). After that, H_R moves to O1, resulting **IM2**. Then, the deuterium is transferred from Glu-172 to C1, leading to the proton exchanged product (the **Pr** state). Finally, **Pr** dissociates from the active site, allowing the enzyme to



Scheme 7. The structures resulted from transferring (a) H_R to Glu-99 from **A** (the **IM1** state), (b) H_R to O1 from **IM1** (the **IM2** state), and (c) the **Pr** state.

start a new catalytic cycle. According to this mechanism, the product will always have the deuterium in the pro-S position, in accordance with the experimental findings [20]. The proposed mechanism in Scheme 8 is slightly different from the mechanism proposed based on QM-cluster calculations [7]. They are the same in all states. However, in the **IM1** state of the QM-cluster based mechanism, H_O is on O1 instead of being on O6.

3.3. Flexibility of the glutamates in the reaction path

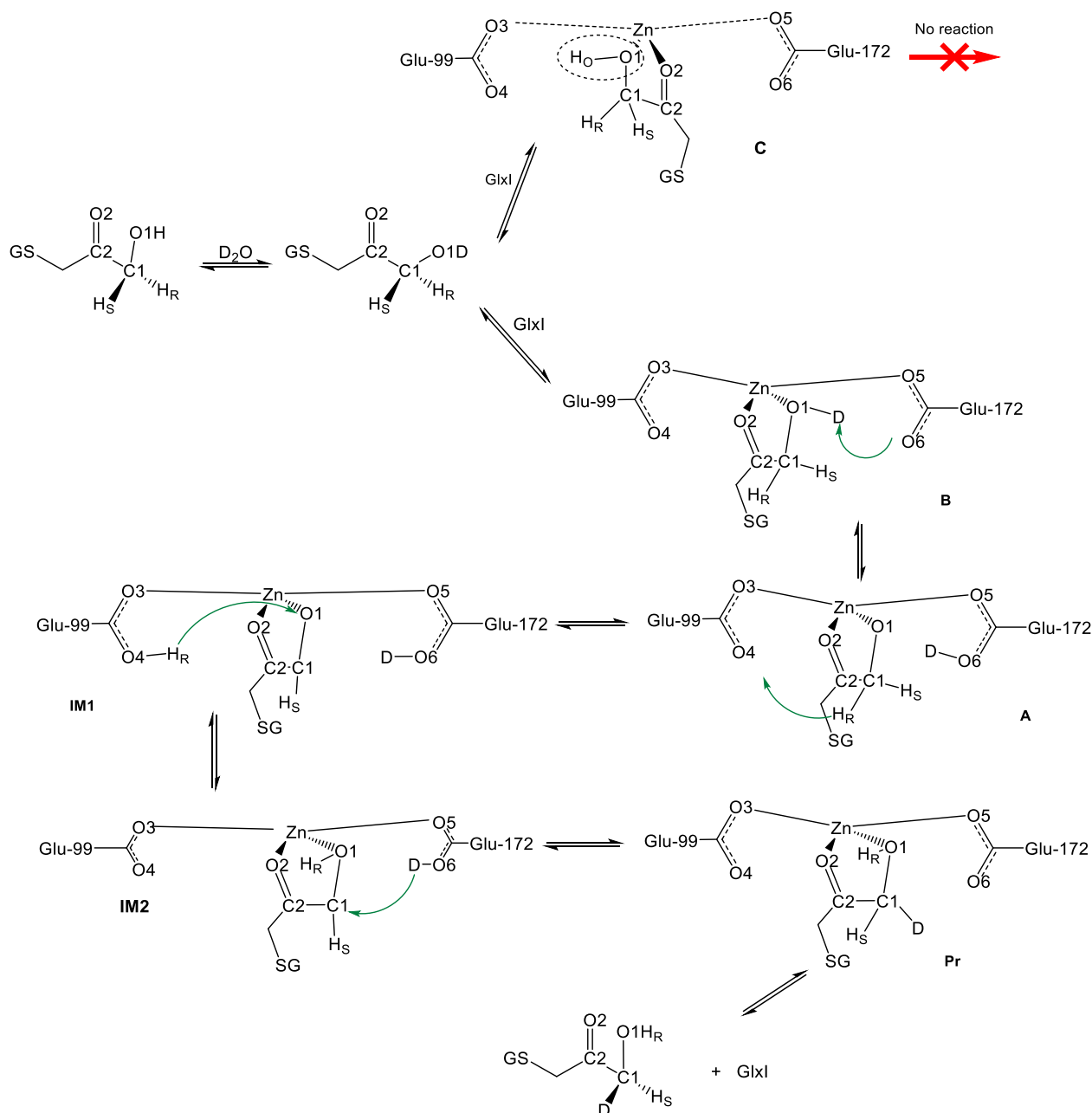
We have previously suggested that the origin of the unusual stereospecificity of GlxI is the higher flexibility of Glu-172 compared to Glu-99 (our molecular dynamics simulations showed that RMSD and RMSF values of Glu-172 are higher than those of Glu-99 and that the flexible loops inside the enzyme are closer to Glu-172) [7]. Here, we have further investigated this hypothesis for the reaction path shown in Scheme 8. We calculated RMSD of heavy atoms of the two active-site

Table 4

RMSD values (in Å) of the heavy atoms of the glutamates during the reaction path shown in Scheme 8 and the average over the path.

	Crystal → B	B → A	A → IM1	IM1 → IM2	IM2 → Pr	Average
Glu-99	0.21	0.08	0.25	0.40	0.15	0.22
Glu-172	0.80	0.11	0.16	0.44	0.24	0.35

glutamate residues in the consecutive QM/MM stationary states (i.e. going from the crystal structure to **B**, from **B** to **A**, from **A** to **IM1**, from **IM1** to **IM2**, and from **IM2** to **Pr**) and collected them in Table 4. We can see that in all steps, except the third one (**A** → **IM1**), the RMSD values of Glu-172 are greater than those of Glu-99. The average RMSDs of Glu-172 is larger than that of Glu-99 along the reaction path (0.35 vs. 0.22 Å; cf. the last column of Table 4). This shows that Glu-172 is more flexible not only in the crystal structure but also along the reaction path.



Scheme 8. Our proposed mechanism for the proton exchange reaction of HOC-SG by GlxI, based on the QM/MM calculations.

4. Conclusions

In this investigation, we have applied classical MD simulations and QM/MM optimizations, together with Big-QM, QM/MM-PBSA and QTCP calculations to study the stereospecific proton exchange of HOC-SG by GlxI. MD simulations with different protonation states of Glu-99, Glu-172 and HOC-SG led to the determination of most stable species. QM/MM results showed that if the substrate binds in the H₀to172 conformation, H₀ is abstracted by Glu-172, whereas if it binds in H₀to99 conformation, H₀ remains on O1 and is directed toward Glu-99.

Our QM/MM results showed that no reaction path from the H₀to99 conformation led to any proton exchange (the key proton transfers were unsuccessful e.g. H₀ to Glu-99). However, for the H₀to172 conformation we found a feasible reaction path (Scheme 8). The results showed that transferring H₀ to the glutamates from the reactant states is the key step to make the proton exchange reaction possible. This proton transfer is spontaneous in the H₀to172 conformation (resulting **A** from **B**), but is not possible for the H₀to99 conformation. Our calculations show that the order of basicity of the substrate and the glutamates is Glu-172 > HOC-SG > Glu-99 (cf. the results in Table 3).

Finally, we also investigated the hypothesis of the higher flexibility of Glu-172 within the reaction path suggested by the QM/MM calculations. The results showed that in the reaction path, the RMSDs of Glu-172 are greater than those of Glu-99. This shows that Glu-172 is more flexible than Glu-99, not only in the crystal structure, but also along the suggested reaction path.

In summary, this and our recent studies on the catalytic mechanism of GlxI [7,10] give the following view of the proton exchange reaction of HOC-SG by GlxI: The active site Zn ion is symmetrically coordinated by Gln-33, His-126, the two active site glutamates and two water molecules before binding any substrate. The substrate analogue binds to the active site displacing the two coordinated water molecules. However, binding HOC-SG in its H₀to172 conformation dissociates Glu-172 from the Zn ion. This takes place by abstracting the alcoholic proton of HOC-SG by Glu-172. On the other hand, for HOC-SG bound in the H₀to99 conformation, nothing happens. This is because Glu-99 is a weaker base than the alcoholic oxygen of HOC-SG and therefore it cannot abstract H₀ and pass it to C1. On the other hand, HOC-SG binds in the H₀to172 conformation and exchanges H₅ by a deuterium from the medium as is shown in Scheme 8.

Acknowledgements

This investigation has been supported by grants from the Swedish research council (projects 2014-5540 and 2018-05003) and from the University of Kurdistan, Sanandaj, Iran (project 96-00036-1). The computations were performed on computer resources provided by the Swedish National Infrastructure for Computing (SNIC) at Lunarc at Lund University and at HPC2N at Umeå University.

Appendix A. Supplementary data

Protonation states of the protein residues in the MD simulations and QM/MM calculations, details of the MD simulations, a restraints file for the Zn-ligand bond restraints in the MD simulations, optimized models used to calculate force constants and charges for the MM force field, MM charges, force constants and restraints used for the Zn clusters, comparison of the forward and backward reaction profiles, details of the QM/MM-PBSA calculations, QM/MM results of ten other QM systems, plots of time dependence of RMSDs of the glutamates in the MD simulations, comparison of the QM/MM, big-QM and QTCP reaction profiles, QTCP free energy profiles for several of the QM systems. Supplementary data to this article can be found online at doi: <https://doi.org/10.1016/j.rechem.2019.100011>.

References

- [1] B.M. Rosner, B. Schink, Purification and characterization of acetylene hydratase of *Pelobacter acetylenicus*, a tungsten iron-sulfur protein, *J. Bacteriol.* 177 (1995) 5767–5772, <https://doi.org/10.1128/jb.177.20.5767-5772.1995>.
- [2] H. Frykman, N. Öhrner, T. Norin, K. Hult, S-ethyl thiooctanoate as acyl donor in lipase catalysed resolution of secondary alcohols, *Tetrahedron Lett.* 34 (1993) 1367–1370, [https://doi.org/10.1016/S0040-4039\(00\)91797-0](https://doi.org/10.1016/S0040-4039(00)91797-0).
- [3] J.A. Landro, E.J. Brush, J.W. Kozarich, Isomerization of (R)- and (S)-glutathiolactaldehydes by glyoxalase I: the case for dichotomous stereochemical behavior in a single active site, *Biochemistry* 31 (1992) 6069–6077, <https://doi.org/10.1021/bi00141a016>.
- [4] M.I. Monterde, M. Lombard, A. Archelas, A. Cronin, M. Arand, R. Furstoss, Enzymatic transformations. Part 58: enantioconvergent biotransformation of styrene oxide derivatives catalysed by the *Solanum tuberosum* epoxide hydrolase, *Tetrahedron Asymmetry* 15 (2004) 2801–2805, <https://doi.org/10.1016/j.tetasy.2004.06.032>.
- [5] M. Kazemi, X. Sheng, W. Kroutil, F. Himmo, Computational study of mycobacterium smegmatis acyl transferase reaction mechanism and specificity, *ACS Catal.* 8 (2018) 10698–10706, <https://doi.org/10.1021/acscatal.8b03360>.
- [6] H.X. Qian, R.Z. Liao, QM/MM study of tungsten-dependent benzoyl-coenzyme A reductase: rationalization of regioselectivity and predication of W vs Mo selectivity, *Inorg. Chem.* 57 (2018) 10667–10678, <https://doi.org/10.1021/acs.inorgchem.8b01328>.
- [7] S. Jafari, N. Kazemi, U. Ryde, M. Irani, Higher flexibility of Glu-172 explains the unusual stereospecificity of glyoxalase I, *Inorg. Chem.* 57 (2018) 4944–4958, <https://doi.org/10.1021/acs.inorgchem.7b03215>.
- [8] A.M. Escorcia, K. Sen, M.C. Daza, M. Doerr, W. Thiel, Quantum mechanics/molecular mechanics insights into the enantioselectivity of the O-acetylation of (R,S)-propanolol catalyzed by candida antarctica lipase B, *ACS Catal.* 7 (2017) 115–127, <https://doi.org/10.1021/acscatal.6b02310>.
- [9] K.D. Dubey, B. Wang, M. Vajpai, S. Shaik, MD simulations and QM/MM calculations show that single-site mutations of cytochrome P450BM3 alter the active site's complexity and the chemoselectivity of oxidation without changing the active species, *Chem. Sci.* 8 (2017) 5335–5344, <https://doi.org/10.1039/c7sc01932g>.
- [10] S. Jafari, U. Ryde, M. Irani, Catalytic mechanism of human glyoxalase I studied by quantum-mechanical cluster calculations, *J. Mol. Catal. B Enzym.* 131 (2016) 18–30, <https://doi.org/10.1016/j.jmolcatb.2016.05.010>.
- [11] A. Maršavelski, M. Močibob, I. Gručić-Sovulj, R. Vianello, The origin of specificity and insight into recognition between an aminoacyl carrier protein and its partner ligase, *Phys. Chem. Chem. Phys.* 17 (2015) 19030–19038, <https://doi.org/10.1039/C5CP03066H>.
- [12] H.J. Wijma, S.J. Marrink, D.B. Janssen, Computationally efficient and accurate enantioselectivity modeling by clusters of molecular dynamics simulations, *J. Chem. Inf. Model.* 54 (2014) 2079–2092, <https://doi.org/10.1021/ci500126x>.
- [13] R.Z. Liao, F. Himmo, Theoretical study of the chemoselectivity of tungsten-dependent acetylene hydratase, *ACS Catal.* 1 (2011) 937–944, <https://doi.org/10.1021/cs200242m>.
- [14] R.-Z. Liao, J.-G. Yu, F. Himmo, Mechanism of tungsten-dependent acetylene hydratase from quantum chemical calculations, *Proc. Natl. Acad. Sci.* 107 (2010) 22523–22527, <https://doi.org/10.1073/pnas.1014060108>.
- [15] B. Kuhn, P.A. Kollman, QM-FE and molecular dynamics calculations on catechol O-methyltransferase: free energy of activation in the enzyme and in aqueous solution and regioselectivity of the enzyme-catalyzed reaction, *J. Am. Chem. Soc.* 122 (2000) 2586–2596, <https://doi.org/10.1021/ja992218v>.
- [16] M. Kazemi, X. Sheng, F. Himmo, Origins of Enantioselectivity of Mycobacterium smegmatis Acyl Transferase: A Computational Analysis, *Chem. – A Eur. J.* 0 (2019). doi:<https://doi.org/10.1002/chem.201902351>.
- [17] S.S. Hall, A.M. Doweyko, F. Jordan, Glyoxalase I enzyme studies. 2. Nuclear magnetic resonance evidence for an enediol-proton transfer mechanism, *J. Am. Chem. Soc.* 98 (1976) 7460–7461. doi:<https://doi.org/10.1021/ja00439a077>.
- [18] R.V. Chari, J.W. Kozarich, Deuterium isotope effects on the product partitioning of fluoromethylglyoxal by glyoxalase I. Proof of a proton transfer mechanism, *J. Biol. Chem.* 256 (1981) 9785–9788. <http://www.jbc.org/cgi/content/long/256/19/9785> (accessed November 1, 2016).
- [19] J.W. Kozarich, R.V.J. Chari, (Glutathionemethyl) glyoxal: mirror-image catalysis by glyoxalase I, *J. Am. Chem. Soc.* 104 (1982) 2655–2657, <https://doi.org/10.1021/ja00373a062>.
- [20] R.V.J. Chari, J.W. Kozarich, Glutathiohydroxyacetone: proton NMR determination of the stereochemistry of proton exchange by glyoxalase I. Evidence for a cis-enediol intermediate based on mirror-image catalysis, *J. Am. Chem. Soc.* 105 (1983) 7169–7171, <https://doi.org/10.1021/ja00362a024>.
- [21] A.D. Cameron, Crystal structure of human glyoxalase I: evidence for gene duplication and 3D domain swapping, *EMBO J.* 16 (1997) 3386–3395, <https://doi.org/10.1093/emboj/16.12.3386>.
- [22] A.D. Cameron, M. Ridderström, B. Olin, M.J. Kavarana, D.J. Creighton, B. Mannervik, Reaction mechanism of glyoxalase I explored by an X-ray crystallographic analysis of the human enzyme in complex with a transition state analogue, *Biochemistry.* 38 (1999) 13480–13490, <https://doi.org/10.1021/bi990696c>.
- [23] I. Feierberg, A.D. Cameron, J. Åqvist, Energetics of the proposed rate-determining step of the glyoxalase I reaction, *FEBS Lett.* 453 (1999) 90–94, [https://doi.org/10.1016/S0014-5793\(99\)00703-6](https://doi.org/10.1016/S0014-5793(99)00703-6).
- [24] M. Ridderström, A.D. Cameron, T.A. Jones, B. Mannervik, Involvement of an active-site Zn²⁺ ligand in the catalytic mechanism of human glyoxalase I, *J. Biol. Chem.* 273 (1998) 21623–21628, <https://doi.org/10.1074/jbc.273.34.21623>.
- [25] U. Richter, M. Krauss, Active site structure and mechanism of human glyoxalase I—an ab initio theoretical study, *J. Am. Chem. Soc.* 123 (2001) 6973–6982, <https://doi.org/10.1021/ja0105966>.

- [26] F. Himo, P.E.M. Siegbahn, Catalytic mechanism of Glyoxalase I: a theoretical study, *J. Am. Chem. Soc.* 123 (2001) 10280–10289, <https://doi.org/10.1021/ja010715h>.
- [27] D.J. Creighton, D.S. Hamilton, Brief history of glyoxalase I and what we have learned about metal ion-dependent, enzyme-catalyzed isomerizations, *Arch. Biochem. Biophys.* 387 (2001) 1–10, <https://doi.org/10.1006/abbi.2000.2253>.
- [28] M. Sousa Silva, A.E.N. Ferreira, R. Gomes, A.M. Tomás, A. Ponces Freire, C. Cordeiro, The glyoxalase pathway in protozoan parasites, *Int. J. Med. Microbiol.* 302 (2012) 225–229, <https://doi.org/10.1016/j.ijmm.2012.07.005>.
- [29] P.E.M. Siegbahn, F. Himo, The quantum chemical cluster approach for modeling enzyme reactions, *Wiley Interdiscip. Rev. Comput. Mol. Sci.* 1 (2011) 323–336, <https://doi.org/10.1002/wcms.13>.
- [30] C.F. Baes, R.E. Mesmer, *The Hydrolysis of Cations*, Wiley, New York, 1976.
- [31] A.C. Aronsson, E. Marmstål, B. Mannervik, Glyoxalase I, a zinc metalloenzyme of mammals and yeast, *Biochem. Biophys. Res. Commun.* 81 (1978) 1235–1240, [https://doi.org/10.1016/0006-291X\(78\)91268-8](https://doi.org/10.1016/0006-291X(78)91268-8).
- [32] M. Srnc, F. Aquilante, U. Ryde, L. Rulišek, Reaction mechanism of manganese superoxide dismutase studied by combined quantum and molecular mechanical calculations and multiconfigurational methods, *J. Phys. Chem. B* 113 (2009) 6074–6086, <https://doi.org/10.1021/jp810247u>.
- [33] J. Heimdal, M. Kaukonen, M. Srnc, L. Rulišek, U. Ryde, Reduction potentials and acidity constants of Mn superoxide dismutase calculated by QM/MM free-energy methods, *ChemPhysChem.* 12 (2011) 3337–3347, <https://doi.org/10.1002/cphc.201100339>.
- [34] M.H.M. Olsson, C.R. Søndergaard, M. Rostkowski, J.H. Jensen, PROPKA3: consistent treatment of internal and surface residues in empirical pK_a predictions, *J. Chem. Theory Comput.* 7 (2011) 525–537, <https://doi.org/10.1021/ct100578z>.
- [35] S. Le Grand, A.W. Götz, R.C. Walker, SPFP: speed without compromise – a mixed precision model for GPU accelerated molecular dynamics simulations, *Comput. Phys. Commun.* 184 (2013) 374–380, <https://doi.org/10.1016/j.cpc.2012.09.022>.
- [36] R. Salomon-Ferrer, A.W. Götz, D. Poole, S. Le Grand, R.C. Walker, Routine microsecond molecular dynamics simulations with AMBER on GPUs. 2. Explicit solvent particle mesh ewald, *J. Chem. Theory Comput.* 9 (2013) 3878–3888, <https://doi.org/10.1021/ct400314y>.
- [37] A.W. Götz, M.J. Williamson, D. Xu, D. Poole, S. Le Grand, R.C. Walker, Routine microsecond molecular dynamics simulations with AMBER on GPUs. 1. Generalized born, *J. Chem. Theory Comput.* 8 (2012) 1542–1555, <https://doi.org/10.1021/ct200909j>.
- [38] D.A. Case, R.M. Betz, D.S. Cerutti, T.E. Cheatham, T.A. Darden, R.E. Duke, T.J. Giese, H. Gohlke, A.W. Goetz, N. Homeyer, S. Izadi, P. Janowski, J. Kaus, A. Kovalenko, T.S. Lee, S. LeGrand, P. Li, C. Lin, T. Luchko, R. Luo, B. Madej, D. Mermelstein, K.M. Merz, G. Monard, H. Nguyen, H.T. Nguyen, I. Omelyan, D.R. Onufriev, D.R. Roe, A. Roitberg, C. Sagui, C.L. Simmerling, W.M. Botello-Smith, J. Swails, R.C. Walker, J. Wang, R.M. Wolf, X. Wu, L. Xiao, P.A. Kollman, AMBER 2016, University of California, (2016). <https://doi.org/10.26434/chemrxiv-2016-14028955>.
- [39] J.A. Maier, C. Martinez, K. Kasavajhala, L. Wickstrom, K.E. Hauser, C. Simmerling, ff14SB: improving the accuracy of protein side chain and backbone parameters from ff99SB, *J. Chem. Theory Comput.* 11 (2015) 3696–3713, <https://doi.org/10.1021/acs.jctc.5b00255>.
- [40] J. Wang, R.M. Wolf, J.W. Caldwell, P.A. Kollman, D.A. Case, Development and testing of a general Amber force field, *J. Comput. Chem.* 25 (2004) 1157–1174, <https://doi.org/10.1002/jcc.20035>.
- [41] W.L. Jorgensen, J. Chandrasekhar, J.D. Madura, R.W. Impey, M.L. Klein, Comparison of simple potential functions for simulating liquid water, *J. Chem. Phys.* 79 (1983) 926–935, <https://doi.org/10.1063/1.445869>.
- [42] L. Hu, U. Ryde, Comparison of methods to obtain force-field parameters for metal sites, *J. Chem. Theory Comput.* 7 (2011) 2452–2463, <https://doi.org/10.1021/ct100725a>.
- [43] C.I. Bayly, P. Cieplak, W. Cornell, P.A. Kollman, A well-behaved electrostatic potential based method using charge restraints for deriving atomic charges: the RESP model, *J. Phys. Chem.* 97 (1993) 10269–10280, <https://doi.org/10.1021/j100142a004>.
- [44] B.H. Besler, K.M. Merz, P.A. Kollman, Atomic charges derived from semiempirical methods, *J. Comput. Chem.* 11 (1990) 431–439, <https://doi.org/10.1002/jcc.540110404>.
- [45] C. Lee, W. Yang, R.G. Parr, Development of the Colle-Salvetti correlation-energy formula into a functional of the electron density, *Phys. Rev. B* 37 (1988) 785–789, <https://doi.org/10.1103/PhysRevB.37.785>.
- [46] A.D. Becke, Density-functional exchange-energy approximation with correct asymptotic behavior, *Phys. Rev. A* 38 (1988) 3098–3100, <https://doi.org/10.1103/PhysRevA.38.3098>.
- [47] A.D. Becke, Density-functional thermochemistry. III. The role of exact exchange, *J. Chem. Phys.* 98 (1993) 5648–5652, <https://doi.org/10.1063/1.464913>.
- [48] S. Grimme, J. Antony, S. Ehrlich, H. Krieg, A consistent and accurate ab initio parametrization of density functional dispersion correction (DFT-D) for the 94 elements H–Pu, *J. Chem. Phys.* 132 (2010) 154104, <https://doi.org/10.1063/1.3382344>.
- [49] S. Grimme, S. Ehrlich, L. Goerigk, Effect of the damping function in dispersion corrected density functional theory, *J. Comput. Chem.* 32 (2011) 1456–1465, <https://doi.org/10.1002/jcc.21759>.
- [50] A. Schäfer, H. Horn, R. Ahlrichs, Fully optimized contracted Gaussian-basis sets for atoms Li to Kr, *J. Chem. Phys.* 97 (1992) 2571–2577, <https://doi.org/10.1063/1.463096>.
- [51] F. Furche, R. Ahlrichs, C. Hättig, W. Klopper, M. Sierka, F. Weigend, Turbomole, *Wiley Interdiscip. Rev. Comput. Mol. Sci.* 4 (2014) 91–100, <https://doi.org/10.1002/wcms.1162>.
- [52] J.M. Seminario, Calculation of intramolecular force fields from second-derivative tensors, *Int. J. Quantum Chem.* 60 (1996) 1271–1277, [https://doi.org/10.1002/\(SICI\)1097-461X\(1996\)60:7<1271::AID-QUA8-3.0.CO;2-W](https://doi.org/10.1002/(SICI)1097-461X(1996)60:7<1271::AID-QUA8-3.0.CO;2-W).
- [53] K. Nilsson, D. Lecerof, E. Sigfridsson, U. Ryde, An automatic method to generate force-field parameters for hetero-compounds, *Acta Crystallogr. - Sect. D Biol. Crystallogr.* 59 (2003) 274–289, <https://doi.org/10.1107/S0907444902021431>.
- [54] E. Sigfridsson, U. Ryde, Comparison of methods for deriving atomic charges from the electrostatic potential and moments, *J. Comput. Chem.* 19 (1998) 377–395, [https://doi.org/10.1002/\(SICI\)1096-987X\(199803\)19:4<377::AID-JCC1>3.0.CO;2-P](https://doi.org/10.1002/(SICI)1096-987X(199803)19:4<377::AID-JCC1>3.0.CO;2-P).
- [55] L. Cao, O. Caldararu, U. Ryde, Protonation states of homocitrate and nearby residues in nitrogenase studied by computational methods and quantum refinement, *J. Phys. Chem. B* 121 (2017) 8242–8262, <https://doi.org/10.1021/acs.jpcc.7b02714>.
- [56] X. Wu, B.R. Brooks, Self-guided Langevin dynamics simulation method, *Chem. Phys. Lett.* 381 (2003) 512–518, <https://doi.org/10.1016/j.cplett.2003.10.013>.
- [57] H.J.C. Berendsen, J.P.M. Postma, W.F. van Gunsteren, A. DiNola, J.R. Haak, Molecular dynamics with coupling to an external bath, *J. Chem. Phys.* 81 (1984) 3684–3690, <https://doi.org/10.1063/1.448118>.
- [58] T. Darden, D. York, L. Pedersen, Particle mesh Ewald: an $N \cdot \log(N)$ method for Ewald sums in large systems, *J. Chem. Phys.* 98 (1993) 10089–10092, <https://doi.org/10.1063/1.464397>.
- [59] J.P. Ryckaert, G. Ciccotti, H.J. Berendsen, numerical integration of the cartesian equations of motion of a system with constraints: molecular dynamics of n-alkanes, *J. Comput. Phys.* 23 (1977) 327–341, [https://doi.org/10.1016/0021-9991\(77\)90098-5](https://doi.org/10.1016/0021-9991(77)90098-5).
- [60] D.R. Roe, T.E. Cheatham, PTRAJ and CPPTRAJ: software for processing and analysis of molecular dynamics trajectory data, *J. Chem. Theory Comput.* 9 (2013) 3084–3095, <https://doi.org/10.1021/ct400341p>.
- [61] U. Ryde, The coordination of the catalytic zinc in alcohol dehydrogenase studied by combined quantum-chemical and molecular mechanics calculations, *J. Comput. Aided Mol. Des.* 10 (1996) 153–164, <https://doi.org/10.1007/BF00402823>.
- [62] U. Ryde, M.H.M. Olsson, Structure, strain, and reorganization energy of blue copper models in the protein, *Int. J. Quantum Chem.* 81 (2001) 335–347, [https://doi.org/10.1002/1097-461X\(2001\)81:5<335::AID-QUA1003>3.0.CO;2-Q](https://doi.org/10.1002/1097-461X(2001)81:5<335::AID-QUA1003>3.0.CO;2-Q).
- [63] U. Ryde, QM/MM calculations on proteins, *Methods Enzymol.* 577 (2016) 119–158, <https://doi.org/10.1016/B.S.MIE.2016.05.014>.
- [64] H.M. Senn, W. Thiel, QM/MM methods for biomolecular systems, *Angew. Chemie - Int. Ed.* 48 (2009) 1198–1229, <https://doi.org/10.1002/anie.200802019>.
- [65] N. Reuter, A. Dejaegere, B. Maigret, M. Karplus, Frontier bonds in QM/MM methods: a comparison of different approaches, *J. Phys. Chem. A* 104 (2000) 1720–1735, <https://doi.org/10.1021/jp9924124>.
- [66] L. Hu, P. Söderhjelm, U. Ryde, On the convergence of QM/MM energies, *J. Chem. Theory Comput.* 7 (2011) 761–777, <https://doi.org/10.1021/ct100530r>.
- [67] D.A. Case, V. Babin, J.T. Berryman, R.M. Betz, Q. Cai, D.S. Cerutti, T.E. Cheatham, T.A. Darden, R.E. Duke, H. Gohlke, A.W. Goetz, S. Gusarov, N. Homeyer, P. Janowski, J. Kaus, I. Kolossváry, A. Kovalenko, T.S. Lee, S. LeGrand, T. Luchko, R. Luo, B. Madej, K.M. Merz, F. Paesani, D.R. Roe, A. Roitberg, C. Sagui, R. Salomon-Ferrer, G. Seabra, C.L. Simmerling, W. Smith, J. Swails, Walker, J. Wang, R.M. Wolf, X. Wu, P.A. Kollman, Amber 14 - University of California, (2014). <https://doi.org/10.26434/chemrxiv-2014-14028955>.
- [68] M. Svensson, S. Humbel, R.D.J. Froese, T. Matsubara, S. Sieber, K. Morokuma, ONIOM: a multilayered integrated MO + MM method for geometry optimizations and single point energy predictions. A test for Diels–Alder reactions and $\text{Pt}(\text{P}(\text{t-Bu})_3)_2 + \text{H}_2$ oxidative addition, *J. Phys. Chem.* 100 (2002) 19357–19363, <https://doi.org/10.1021/jp962071j>.
- [69] L. Cao, U. Ryde, On the difference between additive and subtractive QM/MM calculations, *Front. Chem.* 6 (2018) 89, <https://doi.org/10.3389/fchem.2018.00089>.
- [70] J. Tao, J.P. Perdew, V.N. Staroverov, G.E. Scuseria, Climbing the density functional ladder: nonempirical meta-generalized gradient approximation designed for molecules and solids, *Phys. Rev. Lett.* 91 (2003) 146401, <https://doi.org/10.1103/PhysRevLett.91.146401>.
- [71] K. Eichkorn, O. Treutler, H. Öhm, M. Häser, R. Ahlrichs, Auxiliary basis sets to approximate coulomb potentials, *Chem. Phys. Lett.* 240 (1995) 283–289, [https://doi.org/10.1016/0009-2614\(95\)00621-A](https://doi.org/10.1016/0009-2614(95)00621-A).
- [72] K. Eichkorn, F. Weigend, O. Treutler, R. Ahlrichs, Auxiliary basis sets for main row atoms and transition metals and their use to approximate Coulomb potentials, *Theor. Chem. Accounts Theory, Comput. Model. (Theoretica Chim. Acta)*. 97 (1997) 119–124, <https://doi.org/10.1007/s002140050244>.
- [73] L. Hu, J. Eliasson, J. Heimdal, U. Ryde, Do quantum mechanical energies calculated for small models of protein-active sites converge? *J. Phys. Chem. A* 113 (2009) 11793–11800, <https://doi.org/10.1021/jp9029024>.
- [74] S. Sumner, P. Söderhjelm, U. Ryde, Studies of Reaction Energies in Proteins, *J. Chem. Theory Comput.* 9 (2013) 4205–4214, <https://doi.org/10.1021/ct400339c>.
- [75] L. Hu, P. Söderhjelm, U. Ryde, Accurate reaction energies in proteins obtained by combining QM/MM and large QM calculations, *J. Chem. Theory Comput.* 9 (2013) 640–649, <https://doi.org/10.1021/ct3005003>.
- [76] M. Sierka, A. Hogekamp, R. Ahlrichs, Fast evaluation of the coulomb potential for electron densities using multipole accelerated resolution of identity approximation, *J. Chem. Phys.* 118 (2003) 9136–9148, <https://doi.org/10.1063/1.1567253>.
- [77] M. Von Arnim, R. Ahlrichs, Performance of parallel TURBOMOLE for density functional calculations, *J. Comput. Chem.* 19 (1998) 1746–1757, [https://doi.org/10.1002/\(SICI\)1096-987X\(19981130\)19:15<1746::AID-JCC7>3.0.CO;2-N](https://doi.org/10.1002/(SICI)1096-987X(19981130)19:15<1746::AID-JCC7>3.0.CO;2-N).
- [78] M. Kaukonen, P. Söderhjelm, J. Heimdal, U. Ryde, QM/MM-PBSA method to estimate free energies for reactions in proteins, *J. Phys. Chem. B* 112 (2008) 12537–12548, <https://doi.org/10.1021/jp802648k>.
- [79] L. Hu, M. Farrokhnia, J. Heimdal, S. Shlevy, L. Rulišek, U. Ryde, Reorganization energy for internal electron transfer in multicopper oxidases, *J. Phys. Chem. B* 115 (2011) 13111–13126, <https://doi.org/10.1021/jp205897z>.
- [80] J. Srinivasan, J. Miller, P.A. Kollman, D.A. Case, Continuum solvent studies of the stability of rna hairpin loops and helices, *J. Biomol. Struct. Dyn.* 16 (1998) 671–682, <https://doi.org/10.1080/07391102.1998.10508279>.

- [81] S. Genheden, U. Ryde, The MM/PBSA and MM/GBSA methods to estimate ligand-binding affinities, *Expert Opin. Drug Discov.* 10 (2015) 449–461, <https://doi.org/10.1517/17460441.2015.1032936>.
- [82] M. Kaukonen, P. Söderhjelm, J. Heimdal, U. Ryde, Proton transfer at metal sites in proteins studied by quantum mechanical free-energy perturbations, *J. Chem. Theory Comput.* 4 (2008) 985–1001, <https://doi.org/10.1021/ct700347h>.
- [83] V. Luzhkov, A. Warshel, Microscopic models for quantum mechanical calculations of chemical processes in solutions: LD/AMPAC and SCAAS/AMPAC calculations of solvation energies, *J. Comput. Chem.* 13 (1992) 199–213, <https://doi.org/10.1002/jcc.540130212>.
- [84] T.H. Rod, U. Ryde, Quantum mechanical free energy barrier for an enzymatic reaction, *Phys. Rev. Lett.* 94 (2005) 138302, <https://doi.org/10.1103/PhysRevLett.94.138302>.
- [85] T.H. Rod, U. Ryde, Q.M. Accurate, MM free energy calculations of enzyme reactions: methylation by catechol O-methyltransferase, *J. Chem. Theory Comput.* 1 (2005) 1240–1251, <https://doi.org/10.1021/ct0501102>.
- [86] J. Uranga, P. Mikulskis, S. Genheden, U. Ryde, Can the protonation state of histidine residues be determined from molecular dynamics simulations? *Comput. Theor. Chem.* 1000 (2012) 75–84, <https://doi.org/10.1016/j.comptc.2012.09.025>.